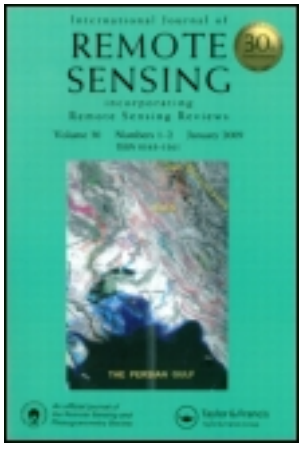

International Journal of Remote Sensing

Publication details, including instructions for authors and subscription information:
http://www.tandfonline.com/loi/tres20

An evaluation of waveband pairs for water column correction using band ratio methods for seabed mapping in the Seychelles

Sarah Hamylton [a] [b]

[a] Department of Geography, University of Cambridge, Cambridge, CB2 3EN, UK

[b] Darwin College, University of Cambridge, Cambridge, CB3 9EU, UK

Available online: 22 Aug 2011

To cite this article: Sarah Hamylton (2011): An evaluation of waveband pairs for water column correction using band ratio methods for seabed mapping in the Seychelles, International Journal of Remote Sensing, 32:24, 9185-9195

To link to this article: http://dx.doi.org/10.1080/01431161.2010.550648

International Journal of Remote Sensing
Vol. 32, No. 24, 20 December 2011, 9185–9195

Taylor & Francis
Taylor & Francis Group

An evaluation of waveband pairs for water column correction using band ratio methods for seabed mapping in the Seychelles

SARAH HAMYLTON*†‡
†Department of Geography, University of Cambridge, Cambridge CB2 3EN, UK
‡Darwin College, University of Cambridge, Cambridge CB3 9EU, UK

(*Received 17 May 2010; in final form 28 November 2010*)

The differential attenuation of visible light (wavelength 400–700 nm) as it travels through the water column confounds the interpretation of remotely sensed imagery acquired over the sea floor. This can be addressed using depth-invariant processing techniques that ratio the radiance values of two wavebands. An evaluation of the performance of different waveband pairs for creating depth-invariant indices of the sea floor is presented. Twenty-eight different band pairs extracted from multispectral Compact Airborne Spectrographic Imager (CASI) data are assessed for the creation of depth-invariant indices over the reef profile of Alphonse Atoll in the Seychelles (water depth 0–30 m). Findings indicate that, for optimal performance, bands selected for depth-invariant processing must be at least 90 nm apart to achieve an optimal ratio of attenuation coefficients within the water column. This optimal ratio must also lie at a central point of the visible spectrum at which longer wavelength bands are not fully attenuated, while shorter wavelength bands exhibit some attenuation over a depth range that coincides with the features of interest in the water column.

1. Introduction

The use of remotely sensed imagery to map benthic marine habitats offers a cost-effective tool for scaling up field survey effort. The radiance levels over water are low compared with those observed over land and the proportion of useful information contained by the signal reaching the sensor is consequently lower for oceanographic remote sensing applications. The major contribution of unwanted noise is the atmosphere, but variations below the water surface in depth, water quality and benthic substrate also influence at-sensor spectral radiance (Holden and LeDrew 2002). These confounding influences on light as it travels through the water column typically arise because of absorption and scattering. Absorption refers to the conversion of electromagnetic energy into other forms, such as heat or chemical energy, whereas scattering is the deflection of electromagnetic radiation as a result of its interaction with the particles (Curran 1985). The attenuation coefficient incorporates both these components to describe the rate at which energy is lost and attenuation length, the inverse of the attenuation coefficient, is the distance over which attenuation is reduced by a factor of e (Rees 1999).

*Email: smh61@cam.ac.uk

International Journal of Remote Sensing
ISSN 0143-1161 print/ISSN 1366-5901 online © 2011 Taylor & Francis
http://www.tandf.co.uk/journals
http://dx.doi.org/10.1080/01431161.2010.550648

Features of primary interest on coral reefs typically occur at water depths of up to 30 m (Done 1983). Differential attenuation of light within this path length through the water column results in both a decreased ability to discriminate between different benthic coverages with increasing depth and different spectra being recorded for the same benthic coverage at different depths. This presents a challenge to the remote sensing of subsurface benthic features, and it is necessary to characterize and correct the effects of the water column on benthic reflection for applications such as the production of habitat maps. The efficacy of compensating for variable attenuation of light in the water column during image acquisition prior to performing classifications of remotely sensed imagery has been demonstrated for benthic assemblages through substantial improvements in classification accuracy (e.g. a 22% increase for airborne multispectral imagery) (Mumby *et al.* 1998).

As higher spatial resolution satellites have offered increasingly precise depictions of subsurface features, water column correction (or depth-invariant processing) techniques have been developed to facilitate the recognition of bottom features. Airborne remote sensors are acquiring increasingly high spatial and spectral resolution imagery across a much wider range of channels. Such data sets extend the options for applying water column correction techniques across multiple permutations of different band combinations. This article explores how band selection determines the outcome of water column correction by evaluating band pairs used in a standard correction algorithm devised by Lyzenga (1978). Evaluations are carried out using a flight strip of data acquired in January 2005 using a Compact Airborne Spectrographic Imager (CASI-1) across the profile of a coral atoll in the Seychelles.

1.1 *The theory of depth-invariant processing*

Depth-invariant processing is commonly carried out in order to interpret optical remotely sensed imagery of the sea floor. Such processing is contingent on approximation of the vertical radiative transfer regime in a water column to a logarithmic decrease in solar radiation with increased path length travelled, as established by Lyzenga (1978) (equation (1)):

$$L_i = L_{si} + a \times r \times e^{(-2k_i z)}, \tag{1}$$

where L_i is the pixel radiance in band i, L_{si} the deep water radiance in band i (atmospheric scattering component), a the refractive transmittance constant, r the bottom reflectance, k_i the water attenuation coefficient in band i and z the depth.

Tropical waters often satisfy the exponential requirement of this approximation, which has been adopted as the basis for water column correction. Where attenuation occurs at known depths, the components of this equation can be rearranged to calculate bottom reflectance. However, most remote sensing campaigns do not acquire the necessary *in situ* data on water depths to do so. Where multiple spectral bands are available, it is possible to circumvent this problem by ratioing benthic radiance data between bands, allowing the unknowns to be cancelled out to leave the ratio of attenuation coefficients. These ratios can be determined by linearizing the radiance of a known substrate across a range of depths with a log transformation ($\ln(L_i)$) and by constructing a bi-plot for two bands (figure 1). If, prior to log transformation, the radiance due to the atmospheric scattering component, L_{si}, is removed from the individual bands, the gradient of such a line represents the ratio of attenuation coefficients.

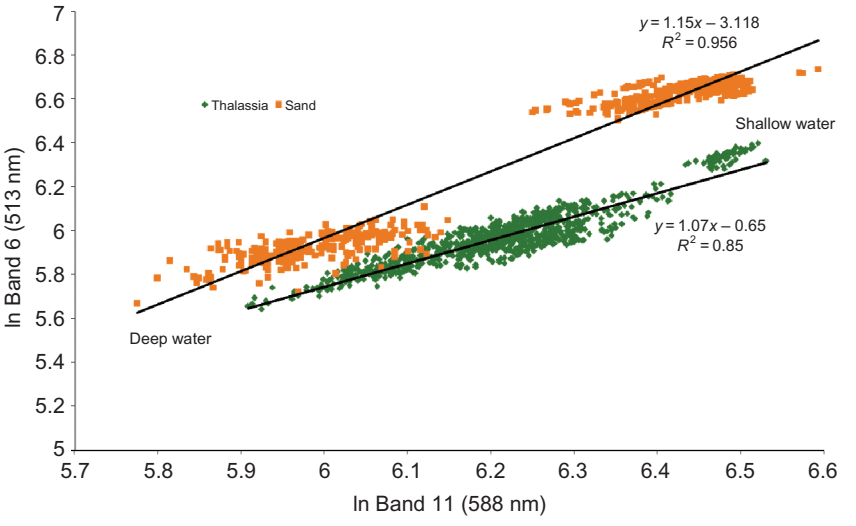

Figure 1. Band ratios of transformed radiance for sand and seagrass pixels across a range of depths. Mid-range spectral wavelengths are 513 nm for band 6 on the *y*-axis and 588 nm for band 11 on the *x*-axis; see table 1 for bandwidths.

If the radiance values for another bottom type are added to the plot, this will produce a similar line with a vertical displacement according to the relative reflectance of the bottom type and a similar gradient (e.g. the gradients of the sand and Thalassia signatures in figure 1 differ by 0.08, ~7% of the slope). This is because the ratio of attenuation coefficients is wavelength-specific. Each *y*-intercept (the point at which the longer wavelength becomes fully attenuated with regard to the shorter) is therefore unique to the bottom type and can be derived using a band pair to represent a single depth-invariant band upon which classification can be performed. Using the equation of a straight line, the *y*-intercept can be calculated for a chosen band pair as follows:

$$\text{Depth invariant index} = \ln(L_i) - \left[\left(\frac{k_i}{k_j}\right) \ln(L_j)\right]. \quad (2)$$

When this is conducted for multiple band pairs (each using different wavelength combinations), a series of depth-invariant bands can be generated and used for image classification. Such a technique requires only knowledge of the locations of a single benthic type across a range of depths as a guide for calibration.

1.2 *Band selection considerations*

In full spatial resolution mode, CASI-1 can record in up to 18 wavelengths in preprogrammed band sets located in the visible section of the electromagnetic spectrum (400–700 nm) at bandwidths ranging from 4.9 to 10.3 nm wide. For the purpose of this study, imagery was acquired across 16 spectral bands at pixel sizes of 1 m^2, yielding coverage of continuous data layers over the area of interest (table 1). The 16-band data set included spectral bands that ranged approximately from 435 to 740 nm, with a loading towards shorter wavelengths that penetrated the water column more effectively.

Table 1. Mid-range wavelengths and bandwidths of the CASI imagery.

Channel	Wavelength (nm)	Bandwidth (nm)
1	434.5	10.3
2	452.0	7.6
3	467.7	6.6
4	481.6	7.6
5	497.3	8.5
6	513.2	7.6
7	528.1	7.6
8	543.0	7.6
9	558.0	7.7
10	573.0	7.7
11	588.0	7.7
12	603.0	7.7
13	634.1	6.8
14	654.9	4.9
15	700.4	4.9
16	740.3	6.8

1.3 *The study site*

Alphonse Atoll, Seychelles (7° 01′ S, 52° 44′ E), lies at the southern end of the Amirantes Ridge on the southwestern margin of the Seychelles Plateau, western Indian Ocean. Alphonse is a symmetrical, triangular atoll (~6 × 4 km along its longest axes; total area 11.3 km^2). The atoll surrounds a large lagoon (5.4 km^2) with a simple dish-shaped morphology that reaches a maximum central depth of 13 m. The subsurface topographic platforms can be described in terms of three distinct zones: a shallow lagoon, an extensive peripheral reef flat (0–3 m water depth) and a steeply sloping outer forereef (5–30 m).

For the purpose of this evaluation, a flight strip of CASI imagery was used that traversed the profile of the atoll (figure 2). This was collected in January 2005 as part of a habitat-mapping campaign that was a joint collaboration between the Khaled bin Sultan Living Oceans Foundation, the Seychelles Ministry of Environment and the Cambridge Coastal Research Unit. The area selected encompassed a range of benthic coverage types across a series of laterally extensive shallow-water platforms spanning a water depth range of approximately 25 m.

2. Methodology: band pair evaluation

For the purpose of implementing Lyzenga's correction model, the objective of band selection is to identify two wavelengths that exhibit attenuation over a water depth range in which the features of interest on coral reefs lie. With 15 water-penetrating bands (≤700 nm) of unique wavelength, 120 potential combinations can be used to carry out the aforementioned analysis. It is therefore useful to guide the selection of appropriate wavelengths by making broad recommendations based on the characteristic physical conditions (attenuation, underwater topography) occurring in a coral reef environment that may influence the correction model. This study evaluated band pairs by selecting pairs that varied in terms of the distance between the two wavelengths selected and the distance between the wavelengths selected and either edge of

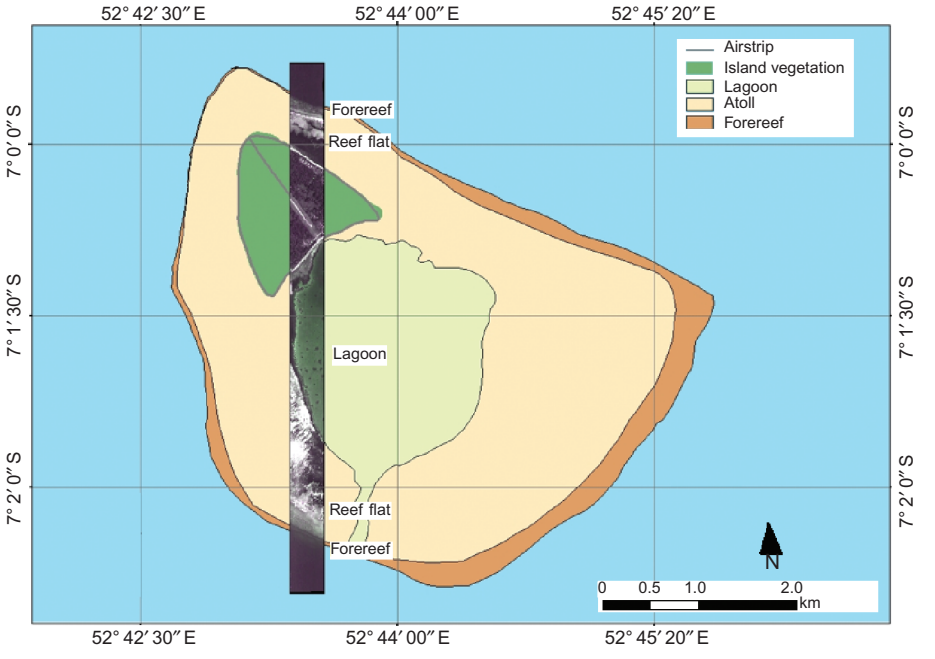

Figure 2. Alphonse Atoll, southern Seychelles, with the strip of CASI imagery superimposed and reef zones labelled.

the optical section of the electromagnetic spectrum. Bands were selected in line with the following three strategies:

(1) **Vary the distance between bands:** Select a band close to the centre of the optical spectrum and, keeping this constant, gradually move its pair towards either end of the sampled spectrum (e.g. 5 vs. 6, 5 vs. 7, 5 vs. 8).
(2) **Vary the distance from the extreme:** Keep sampled bands a constant distance apart and gradually move the pair from one extreme of the spectrum sampled to the other (e.g. 1 vs. 5, followed by 2 vs. 6, 3 vs. 7).
(3) **Vary both distance between bands and distance from the extreme:** Start with the two closest bands in the middle (8 vs. 9) and sample progressively outwards until the two extreme bands were plotted against each other (1 vs. 15).

Band 16 was excluded from the analysis as it measured the radiance at a wavelength that was too long to penetrate water (740 nm). A series of 28 depth-invariant bands was therefore created from multiple band pairs using these strategies. Prior to transformation, the radiance component due to atmospheric scattering was removed from each band. This was achieved by exporting the data of 150 pixels above optically deep water, finding their average value for each wavelength and subtracting this from each band of the image to be corrected. The radiances of 1048 sand pixels falling at a known range of water depths were then exported from the image data, linearized with a natural log transformation and plotted against each other to derive the ratio of attenuation coefficients (gradient). Equation (2) was then applied to each band pair in order to derive a depth-invariant band. A model was developed with an x- and y-stream representing the two wavelengths on the bi-plot (figure 1). This transformed

both the bands, then computed the product of the gradient and transformed longer wavelength data (x-axis) and subtracted this from the shorter wavelength data (y-axis) to find the depth-invariant index (y-intercept) for that particular band pair. The model was developed in ERDAS Model Maker^{TM} (Erdas, Inc., Atlanta, GA, USA), and run for every image pixel across multiple band pairs (table 1) to produce a series of depth-invariant bands. This correction was performed on a masked image with optically deep water and land areas removed.

Each depth-invariant index was then assessed with respect to a number of criteria, including: the calibration parameters used to apply the model, the statistical properties of the resultant index and, based on a visual assessment of the output index image, a qualitative measure of correction performance was assigned (categories: very good, good, moderate, poor and very poor). Calibration parameters recorded included the depth range from which the model calibration pixels were collected and the ratio of attenuation coefficients for each band pair. Statistical properties of the resultant index image included a measure of the index contrast (the standard deviation of the distribution of index pixels across the standard 8-bit greyscale output) and the presence or absence of saturation. Saturation occurs as white or black areas on an index image, caused by either full or zero (i.e. no change) attenuation in one of the image wavebands over the water depth in question. This is detectable on the image histogram as a high frequency of occurrence of white or dark pixels. The presence or absence of saturation at either end of the wavelength spectrum was recorded for each band pair.

2.1 *Assessment of the influence of band pair selection on image classification*

To demonstrate the practical application of the findings, the depth-invariant indices created by the six band pairs judged to provide the best quality outputs were input into a supervised classification (Mather 1999), which was trained using field data. The accuracy of the resultant classification was compared with the field maps generated from the same CASI data set as part of a wider mapping campaign for the Amirantes Islands in which image processing was carried out using all the available CASI wavebands without water column correction (Spencer *et al.* 2009).

3. Results: band pair evaluation

The depth-invariant indices took the form of an 8-bit greyscale image, the values of which for each pixel transitioned from white (255) to black (0) with decreasing albedo of the bottom surface. Bright zones corresponded to sand-dominated areas (e.g. the central lagoonal area of the strip), whereas the presence of live or dead organic matter darkened the index (e.g. coral, seagrass and algae on the reef flat) (figure 3).

For the combination of this oceanic water optical quality and the chosen sand calibration areas, bands with wavelengths approaching the red end of the spectrum (700 nm) became fully attenuated at shallow depths ($\sim$3 m). This limited the depth range from which pixels could be exported to calibrate the correction model, resulting in considerable variation in the number of data points used to estimate the ratio of attenuation coefficients for different depth-invariant indices (table 2).

A consistent trend was observable in which the ratio of attenuation coefficients between band pairs approached 1 as the distance between the selected wavelengths decreased. This was accompanied by a reduction in the contrast of the output index image.

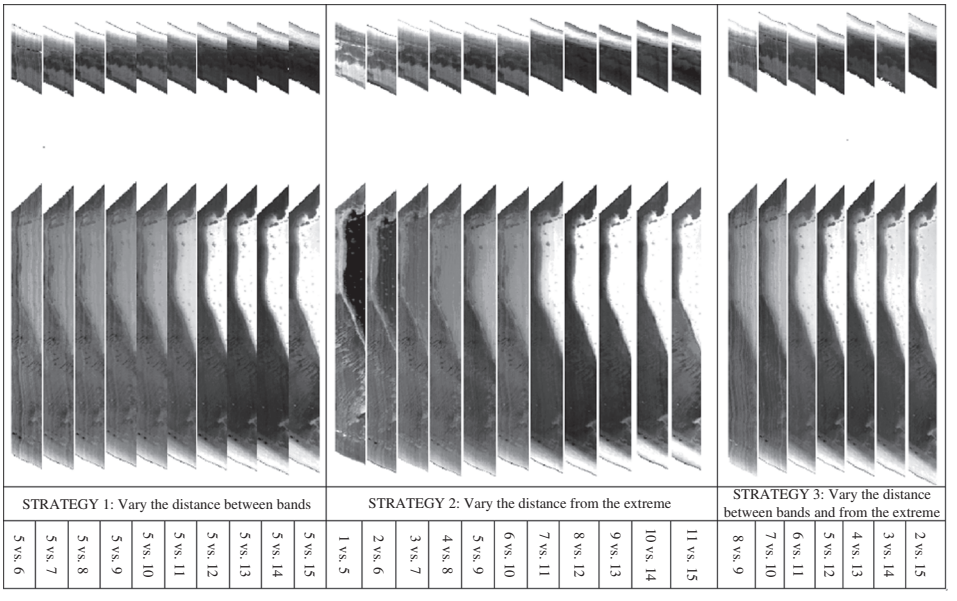

Figure 3. Depth-invariant images produced by using the various waveband pairs in the correction model (central white area represents masked exposed land as depicted in figure 2).

Visual assessments of the quality of depth-invariant indices ranged from very good to very poor, with a tendency for deeper forereef substrate to exhibit white areas on the depth-invariant index, which were caused by saturation at longer wavelengths where light was fully attenuated. Likewise, shallow areas such as the sandy lagoon substrate exhibited black areas where limited attenuation occurred at shorter wavelengths. In shallow areas, bands in the blue region exhibit limited attenuation, resulting in a horizontal bi-plot with a gradient close to 0. Similarly, bands with a shorter attenuation length may become fully attenuated at deeper depths, leaving only the atmospheric component and resulting in a vertically distributed region of saturation on the bi-plot (figure 4). This could be rectified by removing the pixels extracted from substrate calibration areas that lay within these depth ranges from the analysis, but this reduced the depth range over which the model was calibrated (as can be seen in the depth range column of table 2), resulting in an algorithm that was optimized for shallower substrates. In the case of the example shown in figure 4, the comparatively low band 15 signal for the calibration pixels extracted from deeper depths would be corrected to 0, resulting in an area of white on the image, as can be seen from some of the deeper forereef areas in figure 3.

3.1 *Assessment of the influence of band pair selection on image classification*

The classification was performed on the six depth-invariant indices that were deemed to have the best overall outcome on the imagery (5 vs. 10, 5 vs. 11, 2 vs. 6, 3 vs. 7, 6 vs. 11 and 7 vs. 10). The output thematic layer showed considerable detail across a range of depths spanning the reef profile, both in deep forereef areas where the difference between coral and sand was distinguishable and in shallow reef flat areas where the presence of seagrass could be resolved (figure 5(*b*)). This output contained more detail

Table 2. Criteria for the assessment of band pairs.

Selection strategy	Band combination	Mid-band distance	Depth range (m)	Image contrast (SD)	Saturation present/ absent	Ratio of k	Visual assessment
1	5 vs. 6	15.9	19	38.8	A	0.75	G
	5 vs. 7	30.8	18	39.5	A	0.66	G
	5 vs. 8	45.7	16	40.8	A	0.58	G
	5 vs. 9	60.7	14	47.2	A	0.52	G
	5 vs. 10	75.7	13	55.4	A	0.45	G
	5 vs. 11	90.7	12	64.3	A	0.36	G
	5 vs. 12	105.7	11	69.8	P	0.32	M
	5 vs. 13	136.8	9	74.6	P	0.31	P
	5 vs. 14	157.6	6	78.2	P	0.31	P
	5 vs.15	203.1	4	85.4	P	0.30	P
2	1 vs. 5	62.8	21	86.6	P	0.87	VG
	2 vs. 6	61.2	19	84.1	A	1.41	VG
	3 vs. 7	60.4	17	82.3	A	1.61	VG
	4 vs. 8	61.4	16	79.8	A	0.68	G
	5 vs. 9	60.7	14	77.3	A	0.90	G
	6 vs. 10	59.8	13	75.0	A	0.58	G
	7 vs. 11	59.9	12	72.1	A	0.60	M
	8 vs. 12	60	11	69.9	P	1.70	VP
	9 vs. 13	76.1	9	67.0	P	1.25	VP
	10 vs. 14	81.9	7	64.5	P	1.98	P
	11 vs. 15	112.4	3	62.3	P	2.34	P
3	8 vs. 9	15	14	82.6	A	0.91	VP
	7 vs. 10	44.9	13	84.2	A	0.69	P
	6 vs. 11	74.8	12	86.0	A	0.48	G
	5 vs. 12	105.7	11	88.3	A	0.44	P
	4 vs. 13	152.5	8	90.6	A	0.35	P
	3 vs. 14	187.2	6	91.8	A	0.32	VP
	2 vs. 15	248.4	3	93.2	A	0.25	P

Notes: A, absence of saturation; P, presence of saturation. Visual assessment categories: VG, very good; G, good; M, moderate; P, poor; VP, very poor.

than a similar map produced as part of a larger reef habitat-mapping campaign in which all the CASI bands were used with pre-processing that included an atmospheric correction, but no water column correction (figure 5(*c*)). This map resolved less detail for the same area of forereef in terms of seagrass communities within the matrix of sand patches on the upper reef flat and coral communities on the deeper forereef at the northern extent of the classified area. The classification produced using the subset of depth-invariant indices also compared more favourably to a field validation set, with an overall accuracy of 82%, as opposed to 61% for the map that used all the wavebands.

4. Discussion

With respect to strategy 1, which varied the distance between bands selected, the depth-invariant bands that were produced across a smaller wavelength range (i.e. employing channels that were close together) exhibited reduced contrast. This was likely because the bands were subject to similar absorptive and scattering processes, meaning that the ratio of their attenuation coefficients would be close to 1, as can be

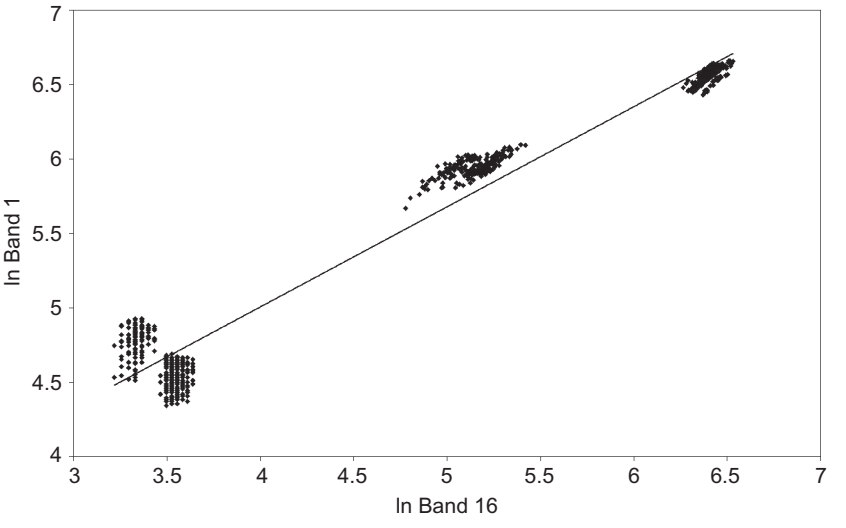

Figure 4. An example bi-plot of band 1 against band 15 to illustrate vertical saturation, the effect of selecting calibration areas deeper than the maximum attenuation length of the longer waveband.

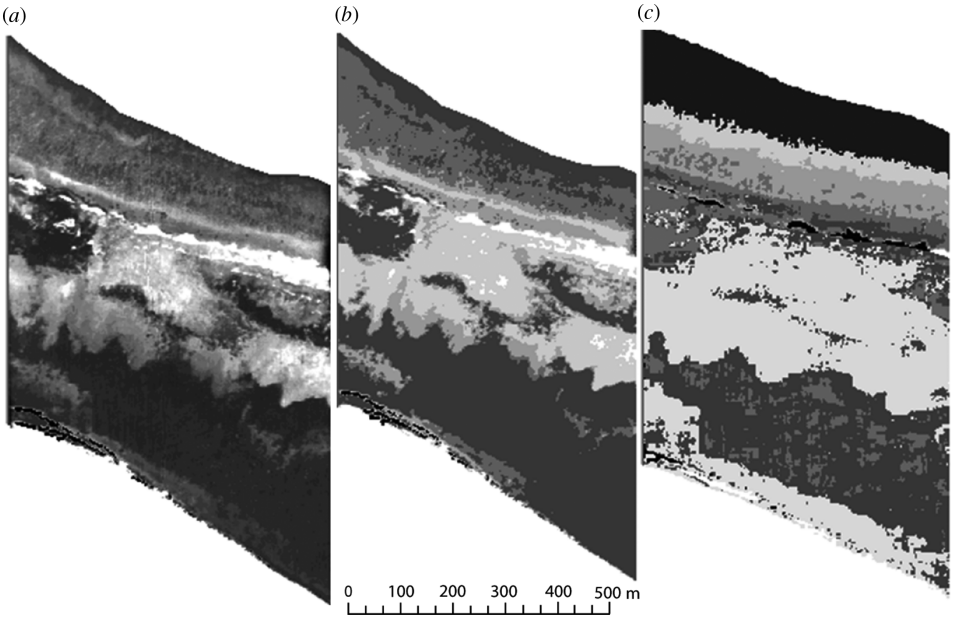

Figure 5. The classification output for a subsection of the study area across the upper reef flat and forereef zones at the top of the image strip: (*a*) the raw image, (*b*) output of a supervised classification on a composite of six depth-invariant indices and (*c*) output of a supervised classification on all the CASI wavebands.

seen by the trend of a decreasing ratio of k with increasing distance between band pairs in table 2. In turn, this would generate a depth-invariant index of limited range (i.e. approximating 0 as the difference between corrected band radiance values was

decreased). It is therefore preferable to maximize the spectral distance between band pairs selected for the creation of depth-invariant indices. However, from the inclusion of band 12 (603 nm) onwards for strategy 1, calibration sand pixels from deeper areas (>12 m) had to be removed due to full attenuation of longer wavelengths. At these longer wavelengths, depth-invariant indices in the lagoon appeared to be saturated, likely because the relative attenuation in the shorter wavelength was much smaller in comparison to the longer wavelength. It is therefore necessary to employ shorter wavelength bands that do not become fully saturated. In the light of these two considerations, the central bands (5 vs. 11) that corresponded to wavelengths around 500–600 nm generated a depth-invariant index that offered the best detail across the depth range of the image. These central bands were placed at a moderate distance apart (~90 nm).

With respect to strategy 2, which moved band pairs iteratively from the blue to red wavelengths, a general trend could be seen whereby the quality of depth-invariant indices decreased as the wavelengths of the bands employed increased. This was likely because of the increased absorption of light at longer wavelengths (Mobley 1994). Shorter wavelength band pairs showed a lot of detail in shallow areas, for example, band pair 1 versus 5 was a notable success on the reef flat where there appeared to be the most detail apparent of all the corrected images. However, the lagoon appeared to be black for this depth-invariant band, due to limited attenuation. In order to derive an accurate ratio of attenuation coefficients, both band pairs need to exhibit some degree of attenuation over the depth range of the calibration pixels selected. Band pair 2 versus 6 (~450 vs. 515 nm) appeared to provide an optimal placement in this respect as both bands were attenuated over a water depth range that covered the features of interest, but did not become fully absorbed (table 2). Longer wavelengths were less successful at distinguishing both shallow and deep features due to attenuation producing white saturation areas on the lower forereef (figure 3). Findings therefore suggested that with respect to strategy 2, short to middle visible wavelength band pairs (450–570 nm) offered the best depth-invariant indices.

Strategy 3 varied both the distance between bands and the distance from the extreme ends of the spectrum. As with the first strategy, reduced contrast was apparent across similar depths in bands that were close together due to their comparable attenuation properties. As the distance between bands was increased, the ratio of k reduced, which increased the contrast of the output depth-invariant index. However, the range of calibration depths was simultaneously reduced as longer wavelength bands subject to absorption were increasingly employed. This resulted in white areas of saturation in the deeper forereef zones. This finding therefore suggested that the central bands, which strike an optimal balance between maximizing the distance between the wavelengths of the bands used and avoiding bands with overly long wavelengths offer better performance, for example, 6 versus 11 (~515–590 nm).

The comparison of classification outputs derived using favourable depth-invariant indices with the approach that indiscriminately utilized all available uncorrected CASI wavebands demonstrated the practical value of these collective strategies. More detail was apparent across the depth range of the study area for the classification that utilized six depth-invariant indices that were optimized in line with the above three strategies. This was also found to correspond more closely to the field data of benthic cover.

5. Conclusion

On the basis of the strategies tested in this article and for the case waters associated with an oceanic atoll environment (i.e. above a forereef, reef flat and lagoon), optimal band pairs met three criteria: (1) they penetrated the water column to a depth range within which the reflectance of a given substrate could be sampled in order to calibrate the model (e.g. they had wavelengths <600 nm); (2) they had an attenuation length that is neither too long nor too short (which results in either vertically or horizontally distributed regions of saturation on the bi-plot, where one band is either fully attenuated with respect to the other or not attenuated at all); and (3) they were not too close together (e.g. at least 90 nm apart). Bands that met all three of these criteria tended to be in moderate positions with regard to the three strategies adopted in this study.

It should be noted that the optimal band pair depends on the depth of features of interest; some may prove favourable for resolving features at one depth but underperform at another. It is therefore difficult to prescribe an overall set of appropriate band pairs for applying Lyzenga's model successfully over large areas that typically encompass wide depth ranges. Nonetheless, the findings of this study provide some useful guidance to be taken into account when processing remotely sensed imagery of shallow water features.

Acknowledgements
The Khaled bin Sultan Living Oceans Foundation and the Great Plains Seychelles are thanked for their assistance with field work and image acquisition at Alphonse Atoll.

References

Curran, P.J., 1985, *Principles of Remote Sensing*, pp. 1–282 (London, UK: Longman Scientific and Technical).

Done, T.J., 1983, Coral zonation: its nature and significance. In *Perspectives on Coral Reefs*, D.J. Barnes and B. Clouston (Eds.), pp. 107–147 (Townsville, Australia: Australian Institute of Marine Science).

Holden, H. and Ledrew, E., 2002, Measuring and modeling water column effects on hyperspectral reflectance in a coral reef environment. *Remote Sensing of Environment*, **81**, pp. 300–308.

Lyzenga, D., 1978, Passive remote sensing techniques for mapping water depth and bottom features. *Applied Optics*, **17**, pp. 379–383.

Mather, P.M., 1999, *Computer Processing of Remotely Sensed Images: An Introduction*, 2nd ed., pp. 1–442 (Chichester, UK: John Wiley & Sons).

Mobley, C.D., 1994, *Light and Water: Radiative Transfer in Natural Waters*, pp. 1–592 (San Diego, CA: Academic Press).

Mumby, P., Clark, C., Green, E. and Edwards, A., 1998, Benefits of water column correction and contextual editing for mapping coral reefs. *International Journal of Remote Sensing*, **19**, pp. 203–210.

Rees, G., 1999, *The Remote Sensing Data Book*, pp. 1–262 (Cambridge, UK: Cambridge University Press).

Spencer, T., Hagan, A.B., Hamylton, S. and Renaud, P., 2009, *Atlas of the Amirantes*, pp. 1–64 (Cambridge, UK: Cambridge University Press).